PERGAMON

International Journal of Heat and Mass Transfer 44 (2001) 1789–1801

International Journal of HEAT and MASS TRANSFER

www.elsevier.com/locate/ijhmt

Conductive heat transport across rough surfaces and interfaces between two conforming media

M.M. Fyrillas *, C. Pozrikidis

Department of Mechanical and Aerospace Engineering, University of California, San Diego, La Jolla, CA 92093-0411, USA

Received 10 November 1999; received in revised form 1 May 2000

Abstract

Conductive heat transport across an isothermal three-dimensional irregular surface into a semi-infinite conductive medium and heat transport across the interface between two semi-infinite conductive media are considered by asymptotic and numerical methods. The temperature profile far from the surface or interface varies in a linear manner with respect to distance normal to the mean position of the surface or interface, and is displaced by a constant with respect to the linear profile corresponding to the flat geometry. The displacement constant amounts to a macroscopic temperature drop or discontinuity that depends on the geometry of the irregularities and on the media conductivities. An asymptotic expansion for the jump is derived by the method of domain perturbation for small-amplitude, doubly-periodic corrugations, and an integral formulation is developed for finite-amplitude corrugations. Numerical results based on the boundary element method for three-dimensional wavy corrugations with square or hexagonal pattern show that the asymptotic results are accurate when the ratio of the vertical span to the wavelength of the corrugations is less than roughly 0.5. Illustrations of the flux distribution over the corrugated surfaces show explicitly a considerable enhancement or reduction at the crests or troughs, even for moderate-amplitude irregularities.

1. Introduction

Consider conductive heat transport from a flat surface located at $z = 0$ over which the temperature is held at the constant value T_0, subject to a fixed rate of transport into the overlying semi-infinite medium. Elementary analysis shows that the temperature profile is given by $T = T_0 + \gamma z$, where the slope $\gamma = -q/\kappa$ is the ratio of the flux q to the medium conductivity κ, e.g., [1]. If the surface is not perfectly flat, a non-linear temperature field is established near the surface, and the temperature profile far from the surface is modified to obtain the shifted linear form

$$T^{\infty} = T_0 + \gamma(c_{\mathrm{D}} + z). \tag{1}$$

The profile displacement constant c_{D}, with units of length, depends on the definition of the origin and, more important, on the surface geometry. The evaluation of c_{D} as a function of the geometry and amplitude of irregularities is necessary for deriving effective boundary conditions to be applied at the nominal position of the planar surface hosting the irregularities.

The problem of transport across an uneven surface described in the preceding paragraph is relevant to a variety of engineering applications involving heat transfer across rough and irregular boundaries, such as the surface of a circuit board in microelectronics. Consider, for example, heat transport from an irregular surface toward a planar surface placed at a distance d above the irregular surface, where the temperature over the planar surface is held constant at the value T^{∞}. If d is sufficiently larger than the amplitude of the corrugations, the heat flux across the planar surface is given by

$$q = -\kappa \frac{T^{\infty} - T_0 - \gamma c_{\mathrm{D}}}{d}. \tag{2}$$

* Corresponding author. Tel.: +1-858-534-6530; fax: +1-858-534-7078.

E-mail addresses: mfyrillas@cytanet.com.cy (M.M. Fyrillas), cpozrikidis@ucsd.edu (C. Pozrikidis).

0017-9310/01/$ - see front matter
PII: S0017-9310(00)00225-8

Nomenclature

$\mathbf{a}_1$, $\mathbf{a}_2$	base vectors describing a doubly-periodic interface
a_{1x}, a_{1y}	components of $\mathbf{a}_1$
a_{2x}, a_{2y}	components of $\mathbf{a}_2$
A	area of a unit cell
$A_{m,n}$	coefficients of the Fourier expansion of the temperature field
$\mathbf{A}^{\mathrm{D}}$	disturbance vector potential
c_{D}	displacement constant
$\hat{c}_{\mathrm{D}}$	dimensionless displacement constant
d	distance between the upper and lower plates
D	one period of the doubly-periodic interface
edt	exponentially decaying terms
$\mathbf{e}_z$	unit vector in the z-direction
$G^{\mathrm{3D-2P}}$	Green's function of Laplace's equation
H	function describing the position of the interface
h_{c}	surface contact conductance
I	imaginary unit
$K(m,n)$	eigenvalues of the Laplacian operator in oblique coordinates
$\mathbf{k}_1$, $\mathbf{k}_2$	reciprocal wave vectors
k_{1x}, k_{1y}	components of $\mathbf{k}_1$
k_{2x}, k_{2y}	components of $\mathbf{k}_2$
L	length scale of corrugations
$\mathbf{n}$	unit vector normal to the interface
q_0, q	heat flux
R_{c}	surface contact resistance
T	temperature
T^{∞}	temperature at the far-field
T_0	temperature of the interface
T^{D}	disturbance component of the temperature field
T^i	ith order expansion of the temperature field
W	function describing the location of the interface with respect to the base vectors
$\tilde{W}$	normalized function describing the position of the interface
x, y	coordinates in the plane of the interface
x_1, y_1	non-orthogonal coordinates
$\mathbf{x}$	position vector
$\mathbf{x}'$	position vector
$\mathbf{x}_0$	position vector
z	coordinate normal to the plane of the interface

Greek symbols

$\alpha_{m,n}$	Fourier components of the interface
γ	ratio of the flux to the medium conductivity
ΔT	macroscopic temperature jump
$\widehat{\Delta T}$	dimensionless temperature jump
ΔT_{c}	temperature rise in the contact zone
ϵ	dimensionless small parameter
ζ	strength of vortex sheet
κ	medium conductivity
λ	ratio of conductivities
ϕ	density of the double-layer potential

Subscripts

1	upper medium
2	lower medium
n, m	the (n,m)th coefficient of the Fourier expansion

Superscripts

0, 1, 2	order of the perturbation expansion
3D–2P	three-dimensional and doubly-periodic
∞	indicates the far-field condition

Substituting $\gamma = -q/\kappa$ and rearranging, we find

$$q = -\frac{\kappa}{1 + c_{\mathrm{D}}/d}\frac{T^{\infty} - T_0}{d}. \tag{3}$$

Anticipating that c_{D} will be negative, we recognize the factor $1/(1 + c_{\mathrm{D}}/d)$ as the enhancement in the flux due to surface roughness. This example illustrates that the determination of c_{D} is necessary for evaluating the rate of transport as a function of the surface geometry.

Consider next conductive heat transport across the interface between two media. If the interface is flat, located at $z = 0$, then the temperature profile is given by $T_1 = T_0 + \gamma z$ on one side, and by $T_2 = T_0 + \lambda\gamma z$ on the other side, where T_0 is the uniform temperature of the interface, $\gamma = -q/\kappa_1$ is the slope of the temperature profile in the upper medium, q is the uniform flux, and λ is the ratio of the conductivities of the two media, defined as $\lambda = \kappa_1/\kappa_2$. These linear distributions satisfy the usual requirement of continuity of temperature and flux across the interface. If, however, the interface is not flat, the temperature distribution far from the interface is modified to become

$$T_1^{\infty} = T_0 + \gamma(z + c_{\mathrm{D}}), \quad T_2^{\infty} = T_0 + \lambda\gamma(z - c_{\mathrm{D}}), \tag{4}$$

where c_{D} is a displacement constant dependent on the interface geometry and ratio of conductivities λ. In particular, when $\lambda = 1$, c_{D} vanishes, and as λ tends to infinity, c_{D} tends to the displacement constant discussed previously for transport across an irregular surface held at a constant temperature. The macroscopic discontinuity in the temperature across the interface is given by

$$\Delta T = T_1^{\infty}(z = 0) - T_2^{\infty}(z = 0) = \gamma c_{\mathrm{D}}(1 + \lambda). \tag{5}$$

The evaluation of c_D as a function of λ and of the interface geometry is necessary for establishing macroscopic boundary conditions for the jump in the temperature across an irregular interface. Conservation of energy requires that the macroscopic flux is continuous across the nominally flat interface.

Our main goal in this paper is to evaluate the constant c_D for the two problems described, for non-planar surfaces with doubly-periodic three-dimensional corrugations. First, we carry out a perturbation expansion for small-amplitude corrugations with sinusoidal shapes. Second, we develop an integral formulation for corrugations with arbitrary amplitude, and present numerical results obtained using a boundary element method. In the integral formulation, the temperature field is expressed in terms of a doubly-periodic array of point-source dipoles, and the wall flux is computed from a complementary single-layer representation. An important aspect of the integral formulation is the use of the doubly-periodic Green's function of Laplace's equation in three dimensions, which is computed in an expedited fashion in terms of Ewald sums. The results illustrate the distribution of the flux over the surfaces and demonstrate explicitly the enhancement or reduction in the flux at the crests and troughs of the periodic waves.

The problem of transport across irregular surfaces and interfaces separating two conforming media considered in this paper is related to the much-studied problem of transport across two solid bodies in imperfect contact, where heat flows from one body to the other, as reviewed most recently by Lambert and Fletcher [2], and discussed in the recent papers by Tio and Toh [3] and Das and Sadhal [4]. Two bodies in contact actually touch only at discrete spots or crests whose surface area depends on the elastic and plastic properties of the materials, as well as on the force by which the bodies are pressed together. The total contact area across which transport occurs is only a fraction of the macroscopically measured nominal surface area of the interface. Because of the reduction in transport area due to imperfect contact, a rise in temperature $\Delta T_c = T_1^\infty(z=0) - T_2^\infty(z=0)$ is established across the contact zone to accommodate the specified macroscopic flux q, where the subscript c denotes the contact zone. In the case of perfect contact on a planar surface, $\Delta T_c = 0$; in the diametrically opposite limit of vanishing contact area due to geometrical exclusion or mismatch, ΔT_c is infinite. In engineering applications, the temperature rise in the contact zone is quantified in terms of the surface contact conductance $h_c \equiv -q/\Delta T_c$ or its inverse contact resistance $R_c \equiv 1/h_c$. A temperature profile displacement constant c_D may be defined by setting $q \equiv -\kappa_1 \Delta T_c/[c_D(1+\lambda)]$ and solving for c_D to obtain $c_D \equiv -\kappa_1 \Delta T_c/[q(1+\lambda)]$, where λ is the ratio of the media conductivities.

In the case of imperfect conduct, the temperature rise ΔT_c and associated displacement length c_D is positive due to a deficiency in the actual transport area, as studied by previous authors. In contrast, in the case of perfect conduct across an irregular interface, the temperature drop ΔT_c is negative due to the enhancement in the actual transport area. Imperfect conduct occurs on a microscopic scale due to the natural roughness of surfaces possibly resembling fractals, as discussed by Majumdar and Tien [5] and Brady and Pozrikidis [6]. Perfect conduct considered in this paper occurs on a microscopic scale when one of the media is a gas or a liquid filling the entire space of the irregularities, and on a large scale when two media are fabricated to be conforming. Thus, the problems of contact conductance and transport across conforming non-planar interfaces are complementary from both a geometrical and physical viewpoint.

Transport across a planar surface or interface with distributed irregularities may be regarded as a local model of transport across a generally curved three-dimensional surface or interface with irregularities whose size is smaller than the local radius of curvature. The effective boundary conditions involve a modified macroscopic wall temperature or discontinuity across an interface that is determined by the local flux and wall roughness; the curvature of the surface or interface may be neglected at this level of approximation. This generalization will be implicit in the following discussion.

2. Problem statement

We consider steady heat conduction through a semi-infinite, homogeneous, and isotropic medium bounded by a doubly-periodic surface, as depicted in Fig. 1(a). The geometry of the surface is described by the two base vectors $\mathbf{a}_1$ and $\mathbf{a}_2$ lying in the xy plane, such that if the surface is described by the equation $z = H(\mathbf{x}')$, where $\mathbf{x}' = (x, y)$, then

$$H(\mathbf{x} + n\mathbf{a}_1 + m\mathbf{a}_2) = H(\mathbf{x}'), \tag{6}$$

where n and m are two integers. To satisfy this periodicity condition, we introduce the reciprocal wave number vectors

$$\mathbf{k}_1 = \frac{2\pi}{A}\mathbf{a}_2 \times \mathbf{e}_z, \quad \mathbf{k}_2 = \frac{2\pi}{A}\mathbf{e}_z \times \mathbf{a}_1, \tag{7}$$

where $A = |\mathbf{a}_1 \times \mathbf{a}_2|$ is the area of the unit cell in the xy plane and $\mathbf{e}_z$ is the unit vector along the z-axis, and express the function $H(\mathbf{x}')$ in the form

$$H(\mathbf{x}') \equiv W(\mathbf{x}' \cdot \mathbf{k}_1, \mathbf{x}' \cdot \mathbf{k}_2), \tag{8}$$

where W is a periodic function with period equal to unity with respect to either one of its two scalar arguments. Without loss of generality, we assume that the average value of W over the xy plane is equal to zero.

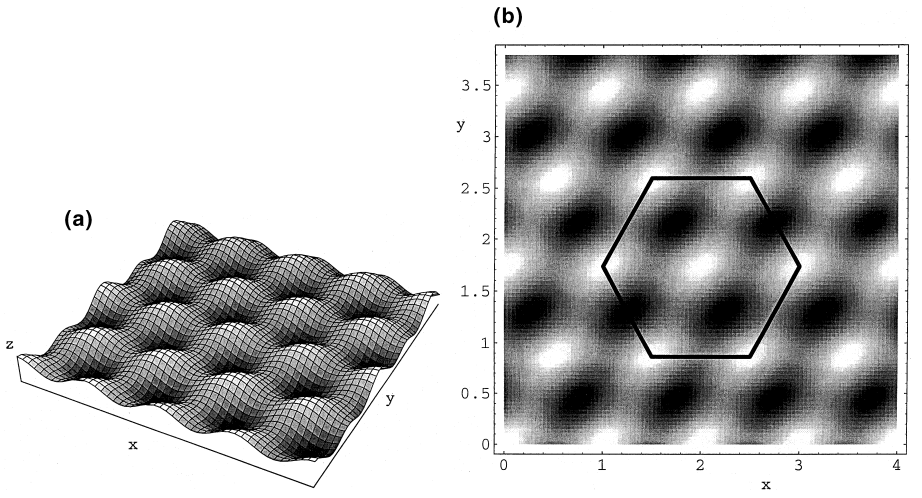

Fig. 1. (a) The geometry of a doubly-periodic surface is determined by the two base vectors $\mathbf{a}_1$ and $\mathbf{a}_2$. When the angle between the two vectors is equal to $\pi/3$, we obtain a hexagonal lattice, as shown in (b) corresponding to $\mathbf{a}_1 = (L, 0)$ and $\mathbf{a}_2 = (0.5L, \sqrt{3}L/2)$, where L is the lattice side.

Steady-state conduction in a homogeneous and isotropic three-dimensional medium is governed by Laplace's equation

$$\nabla^2 T = \frac{\partial^2 T}{\partial x^2} + \frac{\partial^2 T}{\partial y^2} + \frac{\partial^2 T}{\partial z^2} = 0, \tag{9}$$

supplemented with suitable boundary and far-field conditions, e.g., [1]. In this work, we address two different problems distinguished by the choice of boundary conditions.

In the first problem, we consider heat transfer across a periodic surface over which the temperature is held constant at the value T_0. Requiring the Dirichlet boundary condition over the surface, and a uniform rate of transport far from the surface, we obtain the boundary and far-field conditions

$$T\big(z = H(\mathbf{x}')\big) = T_0, \qquad \kappa \frac{\partial T}{\partial z}(z \to \infty) = -q_0, \tag{10}$$

where κ is the medium conductivity. The problem is reduced to solving Laplace's equation (9) subject to conditions (10).

In the second problem, we consider heat transport across a doubly-periodic surface separating two generally different conductive media. Requiring continuity of temperature and flux across the interface, we obtain

$$T_1 = T_2, \qquad \kappa_1 \mathbf{n} \cdot \nabla T_1 = \kappa_2 \mathbf{n} \cdot \nabla T_2, \tag{11}$$

at $z = H(\mathbf{x}')$, where the indices 1 or 2 denote medium 1 or 2, respectively, with medium 1 occupying the semi-infinite space above the interface, and the unit vector $\mathbf{n}$ is normal to the interface. Far from the interface, we specify a constant rate of transport

$$\kappa_1 \frac{\partial T_1}{\partial z}(z \to \infty) = \kappa_2 \frac{\partial T_2}{\partial z}(z \to -\infty) = -q_0. \tag{12}$$

The problem is reduced to solving Laplace's equation (9) subject to the far-field condition (12) and the interfacial conditions (11).

3. Small-amplitude corrugations

For small-amplitude corrugations, an approximate solution to the two problems stated in Section 2 may be found using the method of domain perturbation (Holmes [7]). The idea is to solve Laplace's equation subject to approximate boundary conditions on a flat surface derived by expanding the exact boundary conditions on the corrugated surface in a Taylor series about the planar configuration.

3.1. First problem

First, we consider transport in a semi-infinite domain. Assuming that the amplitude of the corrugations is small, we write

$$\begin{aligned} \mathbf{x}' \cdot \mathbf{k}_1 &= k_{1x} x + k_{1y} y \equiv 2\pi x_1, \\ \mathbf{x}' \cdot \mathbf{k}_2 &= k_{2x} x + k_{2y} y \equiv 2\pi y_1 \end{aligned} \tag{13}$$

and express the function H, defined before in Eq. (6), in the form

$$H(\mathbf{x}') \equiv W = \epsilon \widetilde{W}(2\pi x_1, 2\pi x_2), \tag{14}$$

where ϵ is a small dimensionless number, and the amplitude of $\widetilde{W}$ is of order unity; the periodic function W

was defined in Eq. (8). In terms of the non-orthogonal coordinates x_1 and y_1, Laplace's equation (9) takes the form

$$(k_{1x}^2+k_{1y}^2)\frac{\partial^2 T}{\partial x_1^2}+(k_{2x}^2+k_{2y}^2)\frac{\partial^2 T}{\partial y_1^2} + 2(k_{1x}k_{2x}+k_{1y}k_{2y})\frac{\partial^2 T}{\partial x_1 \partial y_1}+4\pi^2\frac{\partial^2 T}{\partial z^2}=0. \tag{15}$$

Next, we expand T in an asymptotic series in ϵ,

$$T = T^0+\epsilon T^1+\epsilon^2 T^2+\mathcal{O}(\epsilon^3) \tag{16}$$

and the boundary condition expressed by the first of (10), in a Taylor series about $z=0$, to obtain

$$T(z=0)+\epsilon\widetilde{W}(2\pi x_1,2\pi y_1)\frac{\partial T}{\partial z}(z=0) + \frac{\epsilon^2}{2}\widetilde{W}^2(2\pi x_1,2\pi y_1)\frac{\partial^2 T}{\partial z^2}(z=0)+\mathcal{O}(\epsilon^3)=0. \tag{17}$$

Substituting expansion (16) into Eqs. (15) and (17), and setting the sum of coefficients of like powers of ϵ equal to zero, we derive a series of problems.

To zeroth-order, we obtain the flat-surface solution $T^0 = T_0+\gamma z$, where $\gamma=-q_0/\kappa$. To first order, T^1 satisfies Eq. (15) subject to the boundary and far-field conditions

$$T^1(z=0)=-\widetilde{W}\frac{\partial T^0}{\partial z}(z=0)=-\widetilde{W}\gamma, \qquad \frac{\partial T^1}{\partial z}(z\to\infty)=0. \tag{18}$$

To solve this problem, we expand the function $\widetilde{W}$ in a doubly-periodic Fourier series as

$$\widetilde{W}=\sum_{m,n}\alpha_{m,n}\exp[2\pi\mathrm{I}(mx_1+ny_1)], \tag{19}$$

where $\alpha_{m,n}$ are the coefficients of the (m,n) complex–exponential Fourier series, and I is the imaginary unit. To ensure that the mean position of the irregularities is equal to zero, we require $\alpha_{0,0}=0$. A similar expansion for T^1 yields

$$T^1=\sum_{m,n}A^1_{m,n}\exp[-K(m,n)z]\exp[2\pi\mathrm{I}(mx_1+ny_1)]. \tag{20}$$

Substituting expansion (20) into Eq. (15), we find

$$K(m,n)=\sqrt{(k_{1x}^2+k_{1y}^2)m^2+(k_{2x}^2+k_{2y}^2)n^2+2(k_{1x}k_{2x}+k_{1y}k_{2y})nm}. \tag{21}$$

Requiring the boundary condition expressed by the first of Eq. (18), we obtain an expression for the Fourier components, $A^1_{m,n}=-\gamma\alpha_{m,n}$. Because $K_{0,0}=0$, the component $A^1_{0,0}$ leads to a finite value of T^1 in the far field ($z\to\infty$). The displacement constant c_{D} is simply $A^1_{0,0}/\gamma$, which, however, is equal to zero due to the stipulation $\alpha_{0,0}=0$.

The second-order problem for T^2 is governed by Laplace's equation (15) subject to the modified boundary and far-field conditions

$$T^2(z=0)=-\widetilde{W}\frac{\partial T^1}{\partial z}(z=0)-\frac{\widetilde{W}^2}{2}\frac{\partial^2 T^0}{\partial z^2}(z=0) =-\widetilde{W}\sum_{m,n}\alpha_{m,n}\gamma K(m,n)\exp[2\pi\mathrm{I}(mx_1+ny_1)],$$

$$\frac{\partial T^2}{\partial z}(z\to\infty)=0. \tag{22}$$

We note that the right-hand side of the first of Eq. (22) is the product of periodic functions, and this allows us to expand T^2 in a series similar to that for T^1, as shown in Eq. (20).

An explicit expression for T^2 is not necessary for calculating the displacement constant; as in the first-order problem, this is equal to $A^2_{0,0}/\gamma$. The analysis shows that $A^2_{0,0}$ is simply equal to the areal average of the boundary condition over the xy-plane,

$$A^2_{0,0}=\int_0^1\int_0^1 T^2(z=0)\,\mathrm{d}x_1\,\mathrm{d}x_2=-\gamma\sum_{m,n}K(m,n)|\alpha_{m,n}|^2. \tag{23}$$

Expressing the function $\widetilde{W}$ in Fourier sine and cosine components with respect to x and y with coefficients $\beta_{m,n}$, we find

$$c_{\mathrm{D}}=\frac{A^2_{0,0}}{\gamma} =-\frac{\epsilon^2}{2}\left(\sqrt{k_{1x}^2+k_{1y}^2}\sum_m m\beta^2_{m,0}+\sqrt{k_{2x}^2+k_{2y}^2}\sum_n n\beta^2_{0,n}+\frac{1}{2}\sum_{m,n\neq 0}K(m,n)\beta^2_{m,n}\right). \tag{24}$$

Using (7), we find that in terms of the components of the base vectors $\mathbf{a}_1=(a_{1x},a_{1y})$ and $\mathbf{a}_2=(a_{2x},a_{2y})$, the wavenumbers are given by

$$k_{1x}=\frac{2\pi a_{2y}}{A},\quad k_{1y}=-\frac{2\pi a_{2x}}{A},\quad k_{2x}=\frac{2\pi a_{1y}}{A},\quad k_{2y}=-\frac{2\pi a_{1x}}{A}, \tag{25}$$

where $A=|a_{1x}a_{2y}-a_{1y}a_{2x}|$ is the area of the unit cell in the xy plane. Expressions (25) allow us to evaluate the right-hand side of (24). For a rectangular lattice with base vectors along the x and y axes, $a_{1y}=0$, $a_{2x}=0$, we obtain $k_{2x}=0$ and $k_{1y}=0$. For a hexagonal lattice with base vectors $a_{1x}=L$, $a_{1y}=0$, $a_{2x}=0.5L$, $a_{2y}=\sqrt{3}L/2$, where L is a constant length, we obtain $k_{1x}=2/(\pi L)$, $k_{1y}=-2\pi/(\sqrt{3}L)$, $k_{2x}=0$ and $k_{2y}=4\pi/(\sqrt{3}L)$.

Expression (24) provides us with the first term in the expansion of c_{D} with respect to ϵ. In principle, it is

possible to continue the process to compute further terms. In practice, the complexity of the algebraic expressions requires the use of algebraic manipulation programs which lies outside the scope of this work.

3.2. Second problem

The perturbation analysis for the second problem is similar to that for the first problem discussed in the preceding subsection. To each order i in ϵ, the temperature field in the upper or lower medium, T_1 or T_2, satisfies Laplace's equation (15) subject to the following modified interface conditions applied at $z = 0$,

$$\begin{aligned} &T_1^i(z=0) - T_2^i(z=0) = F^i(x_1, y_1), \\ &\kappa_1 \frac{\partial T_1^i}{\partial z}(z=0) - \kappa_2 \frac{\partial T_2^i}{\partial z}(z=0) = G^i(x,y). \end{aligned} \tag{26}$$

The functions $F^i(x,y)$ and $G^i(x,y)$ are obtained by expanding the interface boundary conditions (11) about $z = 0$, substituting the perturbation expansions for T_1 and T_2 into the resulting expressions, and setting the coefficient of each order in ϵ equal to zero.

To zeroth-order, we obtain the flat-interface solution $T_1 = \gamma z$, $T_2 = \lambda\gamma z$, where $\lambda = \kappa_1/\kappa_2$. To first-order, we find that T_1 and T_2 satisfy Eq. (15) subject to the interface conditions

$$\begin{aligned} T_1^1(z=0) - T_2^1(z=0) &= \widetilde{W} \frac{\partial T_2^0}{\partial z}(z=0) - \widetilde{W} \frac{\partial T_1^0}{\partial z}(z=0) \\ &= \gamma(\lambda - 1)\widetilde{W} = \gamma(\lambda-1) \sum_{m,n} \alpha_{m,n} \exp\left[2\pi \mathrm{I}(mx_1 + ny_1)\right] \end{aligned}$$

$$\lambda \frac{\partial T_1^1}{\partial z}(z=0) - \frac{\partial T_2^1}{\partial z}(z=0) = 0, \tag{27}$$

and to the far-field condition

$$\frac{\partial T_1^1}{\partial z}(z \to \infty) = \frac{\partial T_2^1}{\partial z}(z \to -\infty) = 0. \tag{28}$$

As in the first problem, T_1 and T_2 may be expanded in doubly-periodic Fourier series in the form

$$\begin{aligned} T_1^1 &= \sum_{m,n} {}_1A_{m,n}^1 \exp\left[-K(m,n)z\right] \exp\left[2\pi \mathrm{I}(mx_1 + ny_1)\right], \\ T_2^1 &= \sum_{m,n} {}_2A_{m,n}^1 \exp\left[K(m,n)z\right] \exp\left[2\pi \mathrm{I}(mx_1 + ny_1)\right], \end{aligned} \tag{29}$$

where ${}_1A_{m,n}^1$ and ${}_2A_{m,n}^1$ are the Fourier coefficients, and $K(m,n)$ is defined in Eq. (21). Note that these expansions respect the far-field condition (28). Requiring the interface conditions (27), we obtain expressions for the Fourier components,

$${}_1A^1 m,n = \gamma \frac{(\lambda-1)}{1+\lambda} \alpha_{m,n}, \quad {}_2A^1 m,n = -\gamma\lambda \frac{(\lambda-1)}{1+\lambda} \alpha_{m,n}. \tag{30}$$

As in the first problem, the displacement constants c_D for T_1 and T_2 are equal, respectively, to ${}_1A_{0,0}^1/\gamma$ and ${}_2A_{0,0}^1/\gamma$, which vanish because $\alpha_{0,0} = 0$.

The second-order problems for T_1^2 and T_2^2 are governed by Laplace's equation (15) subject to the modified boundary conditions

$$\begin{aligned} &T_1^2(z=0) - T_2^2(z=0) = F^2(x_1, y_1), \\ &\kappa_1 \frac{\partial T_1^2}{\partial z}(z=0) - \kappa_2 \frac{\partial T_2^2}{\partial z}(z=0) = G^2(x,y) \end{aligned} \tag{31}$$

and to the far-field conditions

$$\frac{\partial T_1^1}{\partial z}(z \to \infty) = \frac{\partial T_2^1}{\partial z}(z \to -\infty) = 0, \tag{32}$$

where

$$\begin{aligned} F^2(x_1,y_1) = &- \widetilde{W} \frac{\partial T_1^1}{\partial z}(z=0) - \frac{\widetilde{W}^2}{2} \frac{\partial^2 T_1^0}{\partial z^2}(z=0) \\ &+ \widetilde{W} \frac{\partial T_2^1}{\partial z}(z=0) + \frac{\widetilde{W}^2}{2} \frac{\partial^2 T_2^0}{\partial z^2}(z=0) \\ = &- \gamma \frac{(1-\lambda)^2}{1+\lambda} \widetilde{W} \sum_{m,n} \alpha_{m,n} K(m,n) \\ &\times \exp\left[2\pi \mathrm{I}(mx_1 + ny_1)\right]. \end{aligned} \tag{33}$$

Because we are interested only in the macroscopic temperature jump at the nominal position of the interface, we need only evaluate the difference $\Delta T \equiv {}_1A_{0,0}^2 - {}_2A_{0,0}^2$ which is equal to the areal average of $F^2(x_1,y_1)$, given by

$$\begin{aligned} \int_0^1 \int_0^1 F^2(x_1,y_1)\,\mathrm{d}x_1\,\mathrm{d}x_2 = &-\gamma \frac{(1-\lambda)^2}{1+\lambda} \\ &\times \sum_{m,n} K(m,n) |\alpha_{m,n}|^2. \end{aligned} \tag{34}$$

Expressing the function $\widetilde{W}$ in Fourier sine and cosine series with respect to x and y with coefficients $\beta_{m,n}$, we find

$$\begin{aligned} \Delta T = &-\epsilon^2 \frac{\gamma(1-\lambda)^2}{2(1+\lambda)} \\ &\times \left(\sqrt{k_{1x}^2 + k_{1y}^2} \sum_m m\beta_{m,0}^2 + \sqrt{k_{2x}^2 + k_{2y}^2} \sum_n n\beta_{0,n}^2 + \frac{1}{2} \sum_{m,n \neq 0} K(m,n) \beta_{m,n}^2 \right), \end{aligned} \tag{35}$$

where the wave number components k_{ij} are defined in Eq. (25). The derivation of (35) completes the goal of the perturbation expansion to second order in ϵ.

4. Integral formulation

In Section 3, we derived asymptotic expressions for the displacement constant c_D and for the macroscopic discontinuity across an interface, accurate to second

order with respect to the amplitude of the corrugations. In this section, we develop an integral formulation that expresses the solution in terms of a distribution of point source dipoles, and then compute numerical solutions for arbitrary-amplitude corrugations using a boundary element method.

4.1. First problem

In the first problem, we seek a scalar function T that satisfies Laplace's equation (9) in the upper semi-infinite space confined between positive infinity and the doubly-periodic surface, as illustrated in Fig. 1(a).

As $z \to +\infty$, the requisite harmonic function is required to exhibit the asymptotic behavior

$$T \to T^{+\infty} = \gamma z, \tag{36}$$

where γ is a specified slope. In the first step of the mathematical formulation, T is decomposed into a far-field and a disturbance component designated by the superscript D,

$$T = T^{+\infty} + T^{\mathrm{D}}. \tag{37}$$

As z tends to $+\infty$, the disturbance component T^{D} is required to become constant. The Dirichlet boundary condition expressed by the first of Eq. (10), requires

$$T^{\mathrm{D}} = T_0 - T^{+\infty} \tag{38}$$

over the doubly-periodic boundary.

The disturbance component, T^{D}, is now expressed in terms of a double-layer harmonic potential in the form

$$T^{\mathrm{D}}(\mathbf{x}_0) = \int_D \phi(\mathbf{x})\ \mathbf{n}(\mathbf{x}) \cdot \nabla G^{\mathrm{3D-2P}}(\mathbf{x}, \mathbf{x}_0)\, \mathrm{d}S(\mathbf{x}), \tag{39}$$

where D is one period of the doubly-periodic surface, the point $\mathbf{x}_0$ lies in the solution domain above the doubly-periodic surface, $\mathbf{n}(\mathbf{x})$ is the unit vector normal to D pointing into the upper half-space, and ϕ is the density of the double-layer potential with units of temperature. $G^{\mathrm{3D-2P}}$ is the doubly-periodic Green's function of Laplace's equation in three dimensions discussed by Hautman and Klein [8] and Pozrikidis [9]. As $z \to +\infty$, we obtain the asymptotic behavior

$$\lim_{z_0 \to +\infty} G^{\mathrm{3D-2P}}(\mathbf{x}, \mathbf{x}_0) = -\frac{1}{2A}(z_0 - z) + \mathrm{edt}, \tag{40}$$

where A was defined after Eq. (25), and edt stands for "exponentially decaying terms".

Combining the preceding equations, we find

$$\lim_{z_0 \to +\infty} T = T^{+\infty} + c_{\mathrm{D}} + \mathrm{edt},$$

where

$$c_{\mathrm{D}} = \frac{1}{2A\gamma} \int_D \phi(\mathbf{x}) n_z(\mathbf{x})\, \mathrm{d}S(\mathbf{x}) \tag{41}$$

is the displacement constant expressed as a surface integral of the density of the double-layer potential weighted by the z-component of the normal vector over one period of the surface.

Taking the limit as the point $\mathbf{x}_0$ approaches D, expressing the double-layer integral in terms of its principal value, and using the boundary condition (38), we obtain an integral equation of the second kind for ϕ

$$\phi(\mathbf{x}_0) = -2 \int_D^{\mathrm{PV}} \phi(\mathbf{x})\ \mathbf{n}(\mathbf{x}) \cdot \nabla G^{\mathrm{3D-2P}}(\mathbf{x}, \mathbf{x}_0)\, \mathrm{d}S(\mathbf{x}) + 2[T^{+\infty}(\mathbf{x}_0) - T_0)], \tag{42}$$

where PV denotes the principal value. Having solved the integral equation, we may compute c_{D} using the integral representation (41).

To compute the surface flux, we require the normal derivative of T. This can be found by expressing the gradient of T^{D} in terms of the curl of a disturbance vector potential $\mathbf{A}^{\mathrm{D}}$ as

$$\mathbf{u}^{\mathrm{D}}(\mathbf{x}_0) \equiv \nabla T^{\mathrm{D}}(\mathbf{x}_0) = \nabla \times \mathbf{A}^{\mathrm{D}}(\mathbf{x}_0), \tag{43}$$

e.g., Pozrikidis [10]. The disturbance vector potential is given by the integral representation

$$\mathbf{A}^{\mathrm{D}}(\mathbf{x}_0) = \int_D G^{\mathrm{3D-2P}}(\mathbf{x}, \mathbf{x}_0) \zeta(\mathbf{x})\, \mathrm{d}S(\mathbf{x}), \tag{44}$$

where ζ is the strength of the equivalent vortex sheet given by

$$\zeta = \mathbf{n} \times \nabla \phi \tag{45}$$

involving tangential derivatives of ϕ. The method involves computing ζ from (45), computing $\mathbf{A}^{\mathrm{D}}$ from (44), and then evaluating the normal component of the curl on the right-hand side of (43).

4.2. Second problem

To formulate the second problem, we express the temperature fields in the two media (T_1, T_2) in terms of a double layer potential in the form

$$T_1(\mathbf{x}_0) = \gamma z + \int_D \phi(\mathbf{x})\ \mathbf{n}(\mathbf{x}) \cdot \nabla G^{\mathrm{3D-2P}}(\mathbf{x}, \mathbf{x}_0)\, \mathrm{d}S(\mathbf{x}),$$

$$T_2(\mathbf{x}_0) = \lambda \left(\gamma z + \int_D \phi(\mathbf{x})\ \mathbf{n}(\mathbf{x}) \cdot \nabla G^{\mathrm{3D-2P}}(\mathbf{x}, \mathbf{x}_0)\, \mathrm{d}S(\mathbf{x}) \right). \tag{46}$$

The properties of the double-layer potential ensure that these representations satisfy the flux-continuity condition across the interface required by the second of conditions (11).

Taking the limit as the point $\mathbf{x}_0$ approaches D from above or below, we obtain, respectively,

$$T_+(\mathbf{x}_0)=\gamma z+\frac{1}{2}\phi(\mathbf{x}_0)+\int_D^{\mathrm{PV}}\phi(\mathbf{x})\mathbf{n}(\mathbf{x})\cdot\nabla G^{\mathrm{3D-2P}}(\mathbf{x},\mathbf{x_0})\,\mathrm{d}S(\mathbf{x}),$$
$$T_-(\mathbf{x}_0)=\lambda\left(\gamma z-\frac{1}{2}\phi(\mathbf{x}_0)+\int_D^{\mathrm{PV}}\phi(\mathbf{x})\mathbf{n}(\mathbf{x})\cdot\nabla G^{\mathrm{3D-2P}}(\mathbf{x},\mathbf{x_0})\,\mathrm{d}S(\mathbf{x})\right). \tag{47}$$

Requiring continuity of temperature across the interface, we obtain the following integral equation of the second kind for ϕ

$$\phi(\mathbf{x}_0) = -2\frac{1-\lambda}{1+\lambda}\left(\gamma z+\int^{\mathrm{PV}}\phi(\mathbf{x})\nabla G^{\mathrm{3D-2P}}(\mathbf{x},\mathbf{x_0})\cdot\mathbf{n}(\mathbf{x})\,\mathrm{d}S(\mathbf{x})\right). \tag{48}$$

As $\lambda\to 0$, the ratio $(1-\lambda)/(1+\lambda)$ tends to unity, and (48) reduces to the integral equation (42). As $\lambda\to\infty$, the ratio tends to negative unity, and (48) reduces to the counterpart of the integral Eq. (42) for the lower half-space. To evaluate the macroscopic discontinuity of the temperature across the interface, we work as in the first problem, and find

$$\Delta T=\frac{(1+\lambda)}{2A}\int_D\phi(\mathbf{x})n_z(\mathbf{x})\,\mathrm{d}S, \tag{49}$$

which is the generalized counterpart of (35).

4.3. Numerical method

To solve the integral equations, we discretize one period of the surface D into a collection of curved triangles defined by six nodes, as discussed by Pozrikidis [11]. Triangulation is implemented by successively subdividing an eight-element pattern into a descendent pattern that arises by subdividing each triangle into four descendant triangles. The normal vector and all other variables that undergo a discontinuity across the triangle edges are averaged at the nodes over the host triangles for improved accuracy. All geometrical variables and the unknown functions are approximated with quadratic functions over each triangle with respect to the local triangle coordinates.

The integral equations (42) and (48) are solved by the method of successive substitutions, which involves assuming a form for ϕ, and then recomputing it from the right-hand sides of (42) or (48). It can be shown that the spectral radius of the integral operator on the right-hand side of (42) or (48) is less than unity, and the successive substitutions converge for any surface geometry.

The principal value of the double-layer potential is desingularized with the help of the integral identity

$$\int_D^{\mathrm{PV}}\mathbf{n}(\mathbf{x})\cdot\nabla G^{\mathrm{3D-2P}}(\mathbf{x},\mathbf{x}_0)\,\mathrm{d}S(\mathbf{x})=0, \tag{50}$$

which allows us to write

$$\int_D^{\mathrm{PV}}\phi(\mathbf{x})\,\mathbf{n}(\mathbf{x})\cdot\nabla G^{\mathrm{3D-2P}}(\mathbf{x},\mathbf{x}_0)\,\mathrm{d}S(\mathbf{x}) = \int_D^{\mathrm{PV}}[\phi(\mathbf{x})-\phi(\mathbf{x}_0)]\,\mathbf{n}(\mathbf{x})\cdot\nabla G^{\mathrm{3D-2P}}(\mathbf{x},\mathbf{x}_0)\,\mathrm{d}S(\mathbf{x}). \tag{51}$$

The integral on the right-hand sight of (51) is computed using a seven-point quadrature over each element with respect to the local barycentric triangle coordinates. Most of the computations reported in the next section were carried out using 512 triangles over a period corresponding to 1028 nodes. The results were confirmed to be accurate to at least the third significant figure. Each computation required approximately 30 min of CPU time on a Pentium III 600 MHz running LINUX. The vast majority of the computation time is expended for evaluating the doubly-periodic Green's function.

5. Results

We have evaluated the asymptotic solutions discussed in Sections 2 and 3, and obtained numerical solutions using the boundary element method discussed in Section 4, for surfaces and interfaces hosting doubly-periodic sinusoidal corrugations with square or hexagonal pattern. In the case of the square lattice with side length L, the height of the corrugations is given by

$$H(\mathbf{x}')=\epsilon L\left(\cos\left[\frac{2\pi}{L}x\right]+\cos\left[\frac{2\pi}{L}y\right]\right), \tag{52}$$

where ϵ is the dimensionless amplitude. The vertical distance from a trough to a crest is equal to $4\epsilon L$. In the case of the hexagonal lattice with base vectors $\mathbf{a}_1=L(1,0)$ and $\mathbf{a}_2=L(0.5,\sqrt{3}/2)$, the height of the corrugations is given by

$$H(\mathbf{x}')=\epsilon L\left(\cos\left[\frac{4\pi y}{\sqrt{3}L}\right]+\cos\left[\frac{2\pi x}{L}-\frac{2\pi y}{\sqrt{3}L}\right]\right) \tag{53}$$

and the vertical distance from a trough to a crest is also equal to $4\epsilon L$.

First, we consider the problem of heat transport from an isothermal wavy surface. In Fig. 2(a) and (b), we show graphs of the dimensionless displacement constant $\hat{c}_{\mathrm{D}}=-c_{\mathrm{D}}/L$ plotted against the amplitude of the corrugations ϵ, respectively, for the square and hexagonal pattern. The solid curves represent the asymptotic expression for small amplitudes given in Eq. (24), and the symbols represent numerical results obtained by the boundary element method. The dimensionless displacement constant $\hat{c}_{\mathrm{D}}$ predicted by the perturbation analysis is

$$\hat{c}_{\mathrm{D}}=2\pi\epsilon^2 \quad\text{and}\quad \hat{c}_{\mathrm{D}}=\frac{4\pi}{\sqrt{3}}\epsilon^2 \tag{54}$$

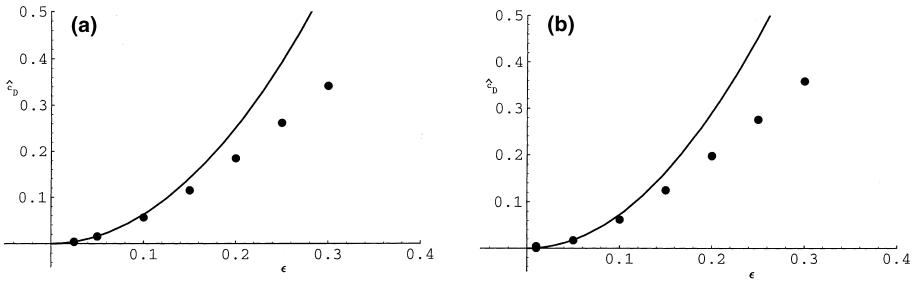

Fig. 2. Displacement constant c_D for (a) the square, and (b) hexagonal lattice. The solid curves represent the prediction of the second-order perturbation expansion given in Eq. (19); the solid circles represent the results of the numerical solution based on the boundary element method.

for the square lattice and the hexagonal lattices, respectively. For small values of ϵ, up to 0.1, the agreement between the asymptotic and numerical results is good, the latter confirming the parabolic behavior near the origin. For higher values of ϵ, the second-order asymptotic theory over-predicts the displacement constant by a substantial amount. The numerical results show that for $\epsilon > 0.15$, c_D increases linearly with ϵ at a rate that depends weakly on the lattice geometry, and is approximately equal to $2/3$.

For large amplitudes ϵ, the temperature distribution near the crests resembles that around a doubly-periodic array of vertical protrusions. Deep down between the protrusions, the temperature tends to become equal to the wall temperature T_0. In the limit of very large amplitude, the protrusions reduce to slender needles.

In Figs. 3 and 4, we present gray-scale graphs of the flux distribution over the surface of the square lattice, and in Figs. 5 and 6, we present corresponding graphs for the hexagonal lattice, for a small and a large amplitude $\epsilon = 0.01$ and 0.3. These results were obtained using the boundary element method. Note that the vertical scale has been compressed to allow for better visibility. For small amplitudes ($\epsilon = 0.01$), corresponding to Figs. 3 and 5, the flux is enhanced at the crests and reduced at the troughs so that its surface integral is constant and equal to γA. Comparisons have shown excellent agreement with the predictions of the asymptotic theory. For high amplitudes ($\epsilon = 0.3$) corresponding to Figs. 4 and 6, the flux distribution appears more intricate. Although maximum heat flux still occurs at the crests, local peaks arise in the intervening space associated with second and higher-order harmonics. A high-order perturbation expansion is necessary to capture the fine features of the distribution using asymptotic methods.

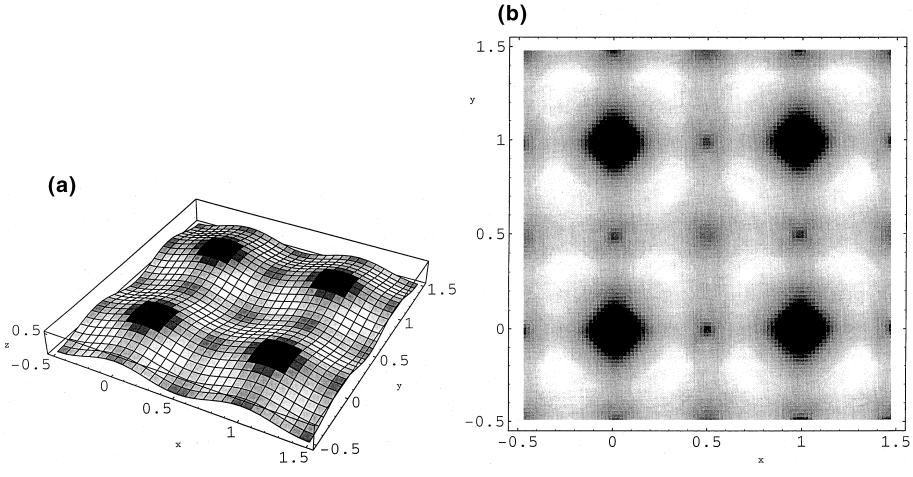

Fig. 3. Flux distribution over the square lattice with small amplitude $\epsilon = 0.01$. Panel (a) shows the surface shaded in gray-scale according to the flux; dark color corresponds to high heat-flux, and light color corresponds to low heat-flux. Note that the vertical scale has been compressed for visibility. Panel (b) is a "topographical map" of the density-flux.

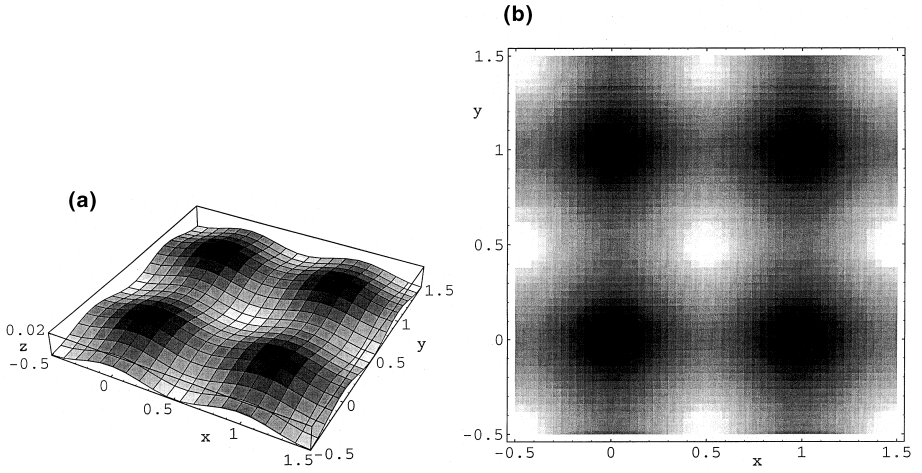

Fig. 4. Similar to Fig. 3 but for a square lattice with amplitude $\epsilon = 0.3$.

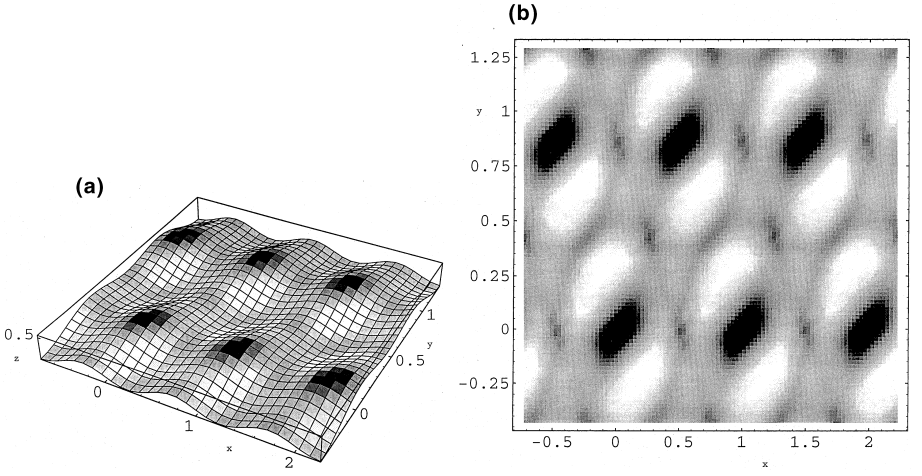

Fig. 5. Similar to Fig. 3 but for a hexagonal lattice with amplitude $\epsilon = 0.01$.

Next, we turn our attention to the second problem of heat transport across a wavy interface. For a wall geometry that is isotropic in the z-direction normal to the unperturbed interface, only values of λ in the range (0,1) need to be considered; the solution for $\lambda > 1$ arises from that for $1/\lambda$ by switching the direction of the z-axis, and setting $\Delta T(\lambda) = \Delta T(1/\lambda)$. In Figs. 7 and 8, we present graphs of the dimensionless macroscopic jump in temperature $\widehat{\Delta T} = -\Delta T/(\gamma L)$ as a function of the conductivity ratio λ, respectively, for the square and hexagonal lattice. The solid curves represent the small amplitude expression for ΔT given by Eq. (35), and the solid circles represent the numerical results. The asymptotic analysis predicts, respectively,

$$\widehat{\Delta T} = 2\pi\epsilon^2 \frac{(1-\lambda)^2}{(1+\lambda)} \quad \text{and}$$

$$\widehat{\Delta T} = 4\pi\epsilon^2 \frac{(1-\lambda)^2}{\sqrt{3}(1+\lambda)}. \tag{55}$$

For small values of ϵ, corresponding to Figs. 7(a) and 8(a), the agreement between the asymptotic and numerical results is exceptional. For larger values of ϵ, (Figs. 7(b) and 8(b)), the relative error appears to be independent of λ at a given amplitude. When $\lambda = 0$, the dimensionless temperature discontinuity reaches a maximum that is equal to the dimensionless displacement constant $\hat{c}_D$ obtained in the first problem Eq. (54).

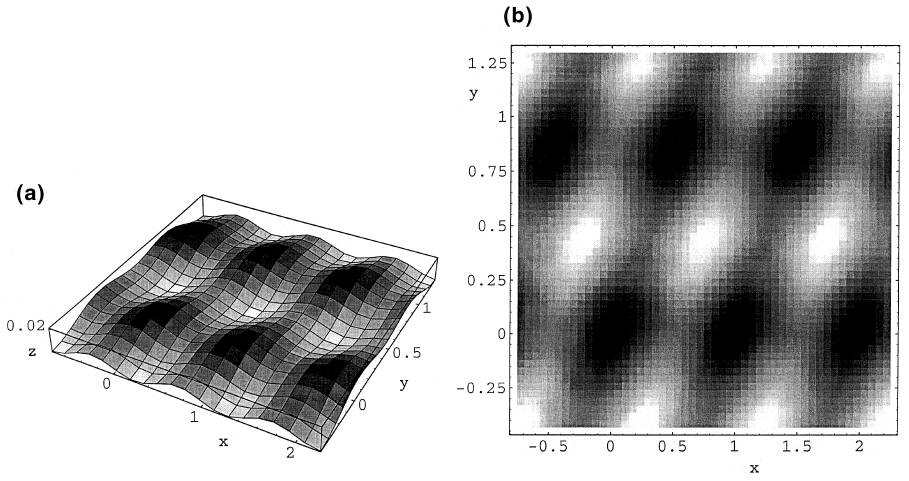

Fig. 6. Similar to Fig. 3 but for a hexagonal lattice with amplitude $\epsilon = 0.3$.

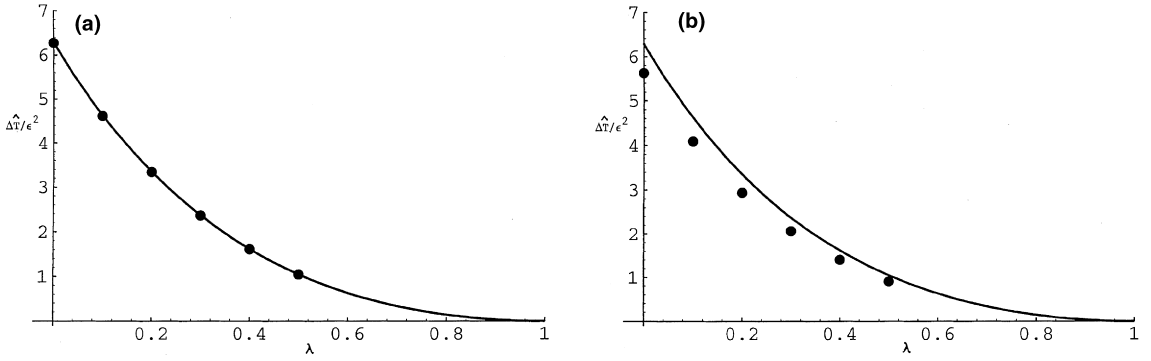

Fig. 7. Dimensionless jump in temperature $\Delta\hat{T}$ plotted against the conductivity ratio λ for square corrugations of amplitude (a) $\epsilon = 0.01$ and (b) 0.1.

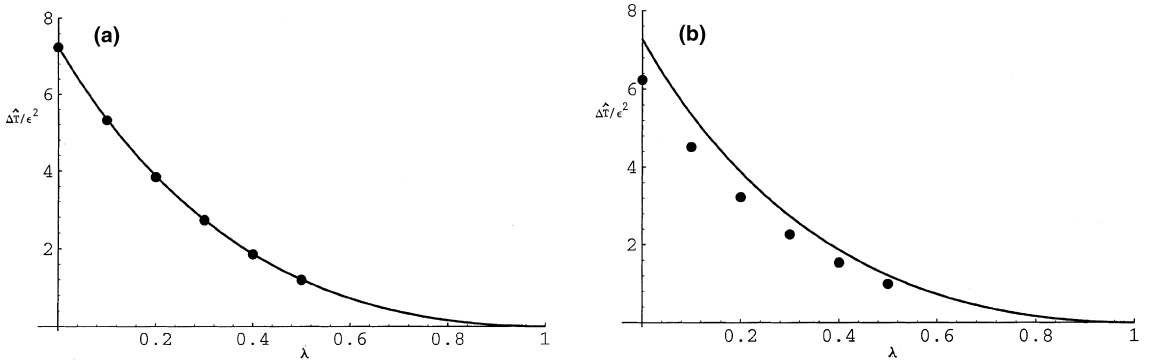

Fig. 8. Dimensionless jump in temperature $\Delta\hat{T}$ plotted against the conductivity ratio λ for hexagonal corrugations of amplitude (a) $\epsilon = 0.01$ and (b) 0.1.

When $\lambda = 1$, i.e., the conductivities of the materials are equal, the temperature field is continuous and $\Delta T = 0$.

6. Discussion

We have addressed two related problems concerning heat transport across irregular surfaces and interfaces between two conducting media. In each case, we evaluated the displacement constant corresponding to the linear field prevailing far from the surface or interface. The theory accounts for surfaces and interfaces of arbitrary geometry and direction of periodicity. The asymptotic expansion is practically limited to surfaces with sinusoidal corrugations, but the integral formulation is able to handle any arbitrary geometries including surfaces with rectangular projections or depressions modeling, for example, microchips placed on boards in microelectronics.

To show the practical application of the results, we consider heat transport across the rough surface of a sphere of radius a representing the surface of a porous particle, held at the constant temperature T_0. Using the first of Eq. (54), we find that the surface flux is given by

$$q = -\kappa \frac{T^\infty - T_0 + 2\pi\epsilon^2 L\gamma}{a}, \tag{56}$$

where T^∞ is the temperature far from the sphere, ϵ is a measure of the surface roughness, and $\gamma = -\partial T/\partial r$ evaluated at $r = a$. Substituting $\gamma = -q/\kappa$ and rearranging, we find

$$q = -\frac{\kappa}{1 - 2\pi\epsilon^2 L/a} \frac{T^\infty - T_0}{a}, \tag{57}$$

where L/a is the ratio between the length scale of the corrugations and the radius of the sphere. The factor $1/(1 - 2\pi\epsilon^2 L/a)$ expresses the enhancement in flux due to surface roughness.

As a second application, we consider heat transport across the rough interface between two slabs, located at $y = a$; the upper slab with conductivity κ_1 extends between $y = a$ and $y = b$, and the lower slab with conductivity κ_2 extends between $y = 0$ and $y = a$, as shown in Fig. 9. Using the first of Eq. (55) we find that the macroscopic discontinuity across the interface is given by

$$\Delta T \equiv T_1(y = a) - T_2(y = a) = -2\pi\epsilon^2 \frac{(1 - \lambda)^2}{1 + \lambda} \gamma L, \tag{58}$$

where $\lambda = \kappa_1/\kappa_2$, $\gamma = -\partial T/\partial y$ at $y = a$ evaluated on the side of the upper slab, and T_1 and T_2 are the macroscopic linear profiles. Setting $q = -\kappa_1(T_U - T_1(y = a))/(b - a) = -\kappa_2(T_2(y = a) - T_L)/a$, substituting $\gamma = -q/\kappa_1$, and assuming for illustration that $b = 2a$, we find

$$q = -\frac{\kappa_1\kappa_2}{\kappa_1 + \kappa_2} \frac{1}{1 - ((2\pi\epsilon^2(1 - \lambda)^2 L)/((1 + \lambda)^2 a))} \times \frac{T_U - T_L}{a}. \tag{59}$$

The second fraction on the right-hand side expresses the enhancement in transport due to the irregularities.

Our results confirm that the enhancement in the rate of transport across a rough surface does not scale with the surface area, but rather with a power of the amplitude of the irregularities. Furthermore, as the amplitude of the irregularities is raised, the enhancement coefficient tends to a finite asymptotic value. Several authors have studied transport across two-dimensional fractal boundaries with infinite surface area [5,6,12] and found that the rate of transport is insensitive to the presence of small scale irregularities beyond a certain level. Although analogous studies for three-dimensional geometries have not been presented, the fast decay of the temperature field within depressions and enclosures is certain to diminish the significance of small scales embedded on larger irregularities.

A large body of experimental data exists on thermal contact conductance, as discussed in the references cited in the introduction. Unfortunately, we were not able to identify analogous data for transport across a nonplanar isothermal surface or an interface between two conformal media, neither we were able to devise a meaningful way of comparing our results with those on

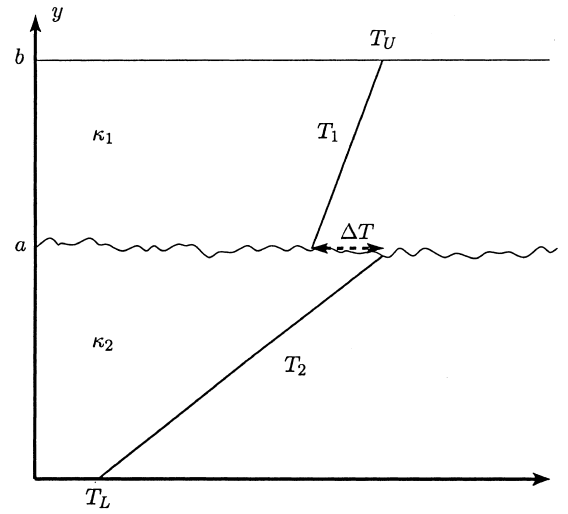

Fig. 9. Conductive heat transport across the rough interface of two slabs with different conductivities. The nominal position of the macroscopically flat interface is located at $y = a$; the upper slab with conductivity κ_1 extends between $y = a$ and $y = b$, and the lower slab with conductivity κ_2 extends between $y = 0$ and $y = a$. At the macroscopic level, the temperature field is discontinuous across the interface, as shown in the figure.

thermal contact conductance. Comparison of our predictions with laboratory data suggests itself as a topic for further research.

Acknowledgements

This work was supported by a grant provided by the National Science Foundation.

References

[1] H.S. Carslaw, J.C. Jaeger, Conduction of Heat in Solids, Clarendon Press, Oxford, 1947.
[2] M.A. Lambert, L.S. Fletcher, Review of models for thermal contact conductance of metals, J. Thermophys. 1 (1997) 129–140.
[3] K.-K. Tio, K.C. Toh, Thermal resistance of two solids in contact through a cylindrical joint, Int. J. Heat Mass Transfer 41 (1998) 1024–2013.
[4] A.K. Das, S.S. Sadhal, Thermal constriction resistance between two solids for random distribution of contacts, Heat Mass Transfer 35 (1999) 101–111.
[5] A. Majumdar, C.L. Tien, Fractal network model for contact conductance, J. Heat Transfer 113 (1991) 516–525.
[6] M. Brady, C. Pozrikidis, Diffusive transport across irregular and fractal walls, Proc. Roy. Soc. London A 442 (1993) 571–583.
[7] M.H. Holmes, Introduction to Perturbation Methods, Springer, Berlin, 1991.
[8] J. Hautman, M.L. Klein, An Ewald summation method for planar surfaces and interfaces, Molecular Phys. 75 (1992) 379–395.
[9] C. Pozrikidis, Conductive mass transport from a semi-infinite lattice of particles, Int. J. Heat Mass Transfer 43 (2000) 493–504.
[10] C. Pozrikidis, Introduction to Theoretical and Computational Fluid Dynamics, Oxford University Press, New York, 1997.
[11] C. Pozrikidis, Numerical Computation in Science and Engineering, Oxford University Press, New York, 1998.
[12] C. Pozrikidis, Unsteady viscous flow over irregular boundaries, J. Fluid Mech. 255 (1993) 11–34.